Acta Crystallographica Section D
Biological Crystallography
ISSN 0907-4449

X-ray structure of a blue copper nitrite reductase at high pH and in copper-free form at 1.9 Å resolution

Mark J. Ellis,[a,b] Fraser E. Dodd,[a] Richard W. Strange,[a] Miguel Prudêncio,[c] Gary Sawers,[d] Robert R. Eady[c] and S. Samar Hasnain[a]*

[a]Synchrotron Radiation Department, CLRC Daresbury Laboratory, Warrington WA4 4AD, England, [b]School of Applied Sciences, De Montfort University, The Gateway, Leicester LE1 9BH, England, [c]Department of Biological Chemistry, John Innes Centre, Colney, Norwich NR4 7UH, England, and [d]Department of Molecular Microbiology, John Innes Centre, Norwich NR4 7UH, England

Correspondence e-mail: s.hasnain@dl.ac.uk

Received 15 January 2001
Accepted 25 May 2001

PDB References: native blue copper nitrite reductase, 1hau; recombinant blue copper nitrite reductase, 1haw.

Copper-containing nitrite reductases possess a trimeric structure where the catalytic Cu site, located at the monomer–monomer interface, resembles the catalytic sites of a number of Zn enzymes. Nitrite reductase from *Alcaligenes xylosoxidans* has optimum activity at pH 5.2 which decreases to a negligible level at pH 8. The structure of this nitrite reductase has previously been determined at pH 4.6. It has now been crystallized under new conditions at pH 8.5. Its crystallographic structure provides a structural explanation for the greatly reduced activity of the enzyme at high pH. Characterization of overexpressed protein in solution by EXAFS suggested that the protein lacked Cu in the catalytic type 2 Cu site and that the site was most probably occupied by Zn. Using the anomalous signals from Cu and Zn, the crystal structure revealed that the expressed protein was devoid of Cu in the catalytic site and that only a trace amount (<10%) of Zn was present at this site in the crystal. Despite the close structural similarity of the catalytic site to a number of Zn enzymes, these data suggest that Zn, if it binds at the catalytic copper site, binds weakly in nitrite reductase.

1. Introduction

Nitrogen is introduced into the biosphere by biological and chemical fixation of dinitrogen (N_2) and removed again by the process of denitrification. Denitrification is the anaerobic respiratory pathway by which some bacteria carry out the sequential reduction of nitrate *via* nitrite, NO and N_2O as intermediates. In addition to the importance of this process in bioenergetics, further impetus for the study of the denitrification process is provided by its environmental impact. This includes the production of NO as a pollutant and N_2O as a potent greenhouse gas, following CO_2 and CH_4 in its contribution to global warming. Dissimilatory nitrite reductase (NiR) is a key enzyme in denitrification since it catalyses the first committed step of denitrification that leads to the gaseous products NO, N_2O or N_2. This results in a significant loss of fixed nitrogen from the terrestrial environment (Payne, 1985; Zumft, 1997)

Two types of NiRs are found in the denitrifying bacteria, the cytochrome cd_1 and copper NiRs (CuNiR); the latter are more widespread, being found in bacteria occupying a greater variety of habitats. The trimeric structures of several CuNiRs have now been established by X-ray crystallography [*Achromobacter cyoclastes* (*Ac*NiR; Godden *et al.*, 1991); *Alcaligenes faecalis* S-6 (*Af*NiR; Kukimoto *et al.*, 1994) and *Alcaligenes xylosoxidans* (*Ax*NiR; Dodd *et al.*, 1998)] and solution X-ray scattering [*Ax*NiR (Grossmann *et al.*, 1993), *Pseudomonas aureofaciens* (*Pa*NiR) and *Af*NiR (Grossmann & Hasnain,

1997)]. The crystal structures of the three CuNiRs show that they are similar, with the monomer consisting of two domains with Greek key β-barrels similar to those found in cupredoxins. Each monomer contains a buried type 1 Cu and a type 2 Cu site located at the monomer–monomer interface. The unusual geometry of type 2 Cu sites has been noted (Murphy *et al.*, 1995) and has been found to be similar to the catalytic metal sites of Zn enzymes including those in carbonic anhydrase (Strange *et al.*, 1995).

Here, we present the crystallographic structures of the high-pH form of native (ntNiR) and recombinant (rcNiR) forms of *Ax*NiR.

2. Materials and methods

2.1. Overproduction of rcNiR in *Escherichia coli*

The overproduction rcNiR in *E. coli* as described by Prudêncio *et al.* (1999) resulted in the isolation of the enzyme with properties indistinguishable from the wild type. The similarity extended to the ready loss of Cu from the type 2 Cu site, as is observed when the enzyme is isolated from *A. xylosoxidans*, unless Cu is added in the initial stages of purification (Abraham *et al.*, 1993). The rcNiR used in this study was atypical in that the protein as isolated had low nitrite reductase activity and contained 0.5 Cu and 2.8 Zn atoms per trimer. The UV-spectral properties were consistent with only a 25% occupancy of the type 1 sites with Cu. The reason for this variation is unclear, but may reflect the availability of Cu to the organism when cultured on a 200 l scale.

2.2. X-ray fluorescence and EXAFS data collection

Trace-element analysis was performed by X-ray fluorescence on EXAFS Station 9.2 at the SRS, Daresbury Laboratory with a 13-element Ge solid-state detector. X-ray absorption spectra at the Cu and Zn *K* edges were measured in fluorescence, again on SRS Station 9.2. Data-collection procedures have been described previously (Murphy *et al.*, 1993). The EXAFS was normalized to a unit metal atom and extracted from the background absorption using the Daresbury Laboratory program *EXBACK* (Morrell *et al.*, 1989). The EXAFS data were analysed using the program *EXCURV*98 (Binsted & Hasnain, 1996).

2.3. Recombinant NiR metal content

Cells with rcNiR were grown using the method of Prudêncio *et al.* (1999) on a 200 l scale. After purification of the protein, analysis of the UV–visible spectrum indicated a ratio of the 280:595 nm peaks of 50:1, when a value of 12:1 was anticipated for the fully Cu-loaded ntNiR. SDS–PAGE gels indicated that the rcNiR had very few contaminants. This suggested that only 25% of the type 1 Cu sites were occupied by Cu.

X-ray fluorescence spectra were measured on a sample of rcNiR at $\sim$60 mg ml^{-1} on SRS Station 9.2 at Daresbury using an incident wavelength of 11 keV and an energy-dispersive multi-element solid-state detector with an energy resolution of $\sim$200 eV. The ratio of the area of the Cu $K\alpha$ peak to the Zn $K\alpha$ peak indicated that there was $\sim$5 times more Zn than Cu in the sample. This was consistent with a trace-metal analysis that indicated the presence of 0.52 Cu and 2.75 Zn atoms per protein molecule, again giving a Zn:Cu ratio of $\sim$5:1. This compares to $\sim$6 Cu atoms per protein molecule for ntNiR (Abraham *et al.*, 1997).

2.4. Protein crystallization

The ntNiR used for crystallization was purified by the method of Abraham *et al.* (1993). rcNiR was prepared as described in Prudêncio *et al.* (1999), with a culture volume of 200 l. Single crystals were grown by the hanging-drop vapour-diffusion method using 25–30% PEG 4K, 0.1 *M* $MgCl_2$ and 0.1 *M* Tris–HCl pH 8.5 with protein concentrations of $\sim$5 mg ml^{-1}. The drops consisted of 3 µl reservoir and protein solutions. The ntNiR and rcNiR crystals were grown at 277 K. All the crystals grew as hexagonal prisms, with the ntNiR being 100 µm thick and 500 µm long and the rcNiR being 300 µm thick and 1 mm long. Although the initial rcNiR protein was blue in colour (*cf.* 280:595 nm ratio of 50:1) the crystals appeared colourless, despite their additional thickness, suggesting that autoreduction of the type 1 Cu site had occurred or that the copper was missing.

2.5. Crystallographic data collection and processing

Data from both ntNiR and rcNiR were collected on beamline BL 6A-2 at the Photon Factory, KEK using the Weissenberg technique (Sakabe, 1991) with Fuji image plates (200 × 400 mm) (Miyahara *et al.*, 1986) and a Fuji BAS2000 scanning system. An X-ray wavelength of 1.0 Å was used for both ntNiR and rcNiR data collections. A second data set was collected for the rcNiR at a wavelength of 1.33 Å to exploit differential changes in the anomalous scattering of Cu and Zn. The crystal orientation and data integration were performed using *DENZO* (Otwinowski & Minor, 1997). Post-refinement was carried out in *SCALEPACK*. The data were then scaled and merged using the *CCP*4 program suite (Collaborative Computational Project, Number 4, 1994).

All crystals were in a hexagonal space group. The unit-cell parameters of the ntNiR protein were $a = b = 81.0$, $c = 99.8$ Å, close to the pH 5.2 structure values $a = b = 81.2$, $c = 100.0$ Å (Dodd *et al.*, 1998). The rcNiR was found to have different unit-cell parameters, namely $a = b = 106.1$, $c = 63.6$ Å. The space group of both crystal forms was $P6_3$ as in the pH 5.2 structure and as anticipated the unit-cell packing is similar. The solvent contents were 59% for the ntNiR and 62% for the rcNiR crystals, respectively. Details of the data processing are shown in Table 1.

2.6. Anomalous maps

Data were collected from rcNiR at two different wavelengths. The first data set was collected at 1.00 Å, above both the Zn and Cu absorption edges, giving anomalous data with Cu f'' = 2.3 e and Zn f'' = 3.2 e. The second, at 1.33 Å, is between the Cu and Zn absorption edges, giving anomalous data with Cu f'' = 3.6 e and Zn f'' = 0.6 e. Anomalous differ-

Table 1
Data statistics.

Values in parentheses are for the outer resolution shell, 2.0–1.9 Å.

	ntNiR	rcNiR	rcNiR†
X-ray wavelength (Å)	1.00	1.00	1.33
Space group	$P6_3$	$P6_3$	$P6_3$
Resolution (Å)	1.9	1.9	1.9
Unit-cell parameters (Å)	$a = b = 89.0$, $c = 99.8$	$a = b = 106.1$, $c = 63.7$	$a = b = 106.1$, $c = 63.6$
Observed reflections	87968 (10194)	133607 (9181)	64606 (8978)
Unique reflections	26943 (3559)	29659 (3854)	27541 (3842)
Completeness (%)	92.3 (83.9)	93.1 (83.4)	87.2 (83.2)
$R_{\rm merge}$ (%)	5.9 (31.0)	6.7 (32.7)	5.6 (32.8)
$I/\sigma(I)$ (%)	10.8 (2.4)	6.1 (2.2)	11.4 (2.2)
Wilson B factor (Å^2)	11.2	15.7	15.0

† This data set was used for calculation of anomalous maps.

ence maps were calculated for both data sets (Figs. 1*a* and 1*b*). The 1.00 Å data gave a weak anomalous peak at the type 1 site, with a very weak peak at the type 2 site. The 1.33 Å data gave a peak at the type 1 site which was stronger than that for the 1.00 Å data. The type 2 site did not exhibit any peak. This is consistent with Cu being present in the type 1 site and only a trace amount of Zn being in the type 2 site. For comparison, anomalous difference maps were calculated for the ntNiR data collected at 1.00 Å (Fig. 1*c*). These data gave much stronger anomalous signals at the Cu sites. This demonstrates that the rcNiR must contain metals substantially below full occupancy, since both Cu and Zn have significant anomalous scattering at this wavelength.

2.7. Structure determination

The structures were solved by molecular replacement using *AMoRe* (Navaza, 1994) using the 2.1 Å refined structure of the pH 5.2 form of *Ax*NiR (Dodd *et al.*, 1998). In the ntNiR case the solution was found directly, with rigid-body refinement giving an R factor of the model of 15.5% and a correlation coefficient of 93.9%.

In the rcNiR case a molecular-replacement solution was not found immediately. Despite a strong rotation-function solution, the translation-function solution was unexpectedly poor with a modest R factor of 42%. Rigid-body refinement did little to reduce this high value. Given the low visible absorbance of rcNiR (∼25% of ntNiR) it might be expected that the type 1 Cu site would have low occupancy. When the metals were removed from the model a satisfactory solution emerged, with the translation function yielding an R factor of 24.8%. Rigid-body refinement reduced this to 22.9% with a correlation coefficient of 87.6. Examination of the solution revealed that the crystal symmetry generated the NiR trimer, with two trimers in the unit cell. Good packing was observed with no clashes between the molecules.

2.8. Refinement

Prior to refinement a set of reflections was set aside for cross-validation ($R_{\rm free}$) purposes. In the case of ntNiR data the $R_{\rm free}$ flags were transferred from the data used in the low-pH NiR refinement (Dodd *et al.*, 1998). As the resolution limit of the ntNiR data was at a higher resolution than the low-pH data, 5% of reflections in the additional resolution shell were added to the $R_{\rm free}$ set. Since the unit cell in the rcNiR is

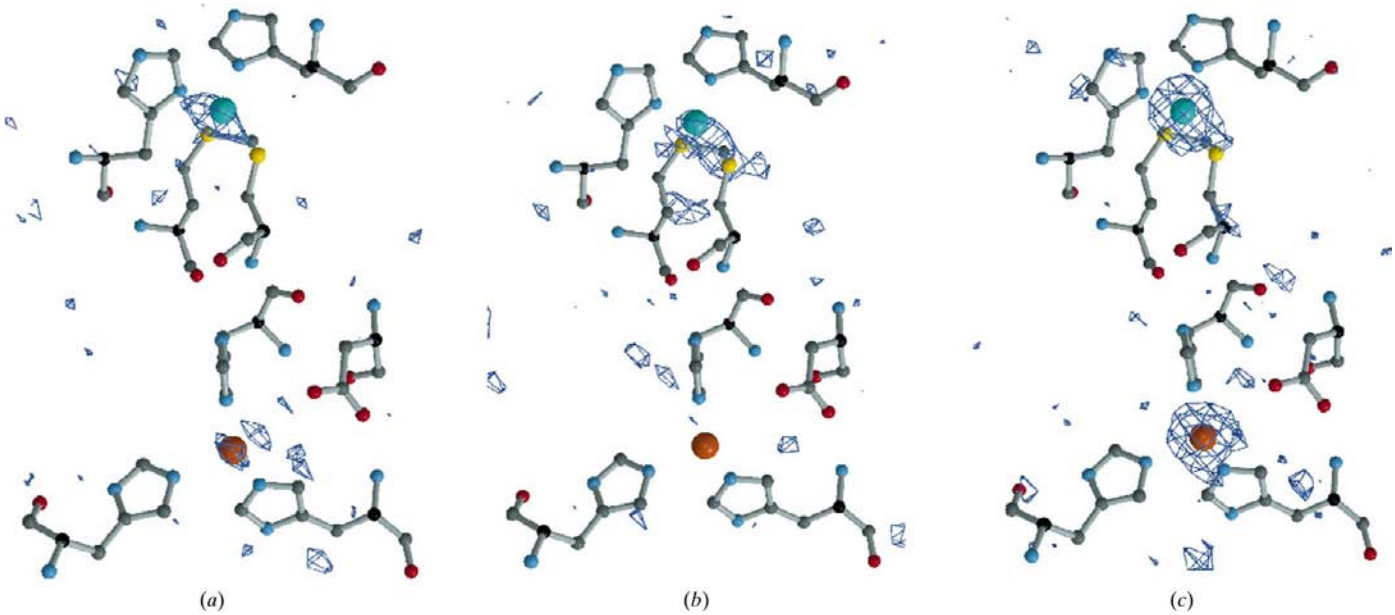

Figure 1
Anomalous difference maps calculated at 4σ for rcNiR at (*a*) 1.00 Å (above the Cu and Zn *K* edges) and (*b*) 1.33 Å (below the Zn but above the Cu edge). The 1.00 Å data show a weak anomalous peak at the type 1 site (5.4σ), with a significantly weaker peak (4.4σ) at the type 2 site. The 1.33 Å data show an enhanced peak at the type 1 site (6.2σ), with a reduction/absence at the type 2 site. This is consistent with Cu being present in the type 1 site and a very small amount of Zn being in the type 2 site. For comparison an anomalous map of ntNiR at 1.00 Å (*c*) is shown where the anomalous peaks are at 18σ and 15σ for the type 1 and type 2 sites, respectively.

Table 2
Refinement statistics.

	ntNiR	rcNiR
R factor (%)	15.5	17.2
R_{free} (%)	19.0	20.0
No. of reflections	26926	29633
No. of parameters	10760	10404
No. of atoms		
Protein	2501	2451
Water	187	149
Metal	2	0.25
B factors		
Protein (Å^2)	17.9	26.4
Water (Å^2)	29.6	34.7
RMS deviations		
Bond distances (Å)	0.013	0.012
Bond angles (°)	1.8	1.8
Peptide planes (°)	0.024	0.024
Aromatic planes (°)	0.012	0.011
Ramachandran plot (non-Gly and non-Pro)		
Residues in most favoured regions (%)	90.9	89.9
Residues in additional allowed regions (%)	9.1	10.1
Overall *G* factor †	−0.11	−0.08

† The *G* factor is a log-odds score based on the observed distributions of stereochemical parameters (Laskowski *et al.*, 1993).

different from the low-pH NiR structure new R_{free} flags were assigned. These constituted 5% of the data (~1000 reflections). All structures were refined using *REFMAC* (Murshudov *et al.*, 1997).

2.8.1. Native structure. The ntNiR model was subjected to cycles of positional and individual *B*-factor refinement in *REFMAC* using data in the resolution range 20.0–1.9 Å. This resulted in a minimal drop in the *R* factor to 15.4% (R_{free} 18.8%). The model consisted of 2527 protein atoms, 179 waters and two Cu atoms. The model was then examined in *O* (Jones *et al.*, 1991) and necessary adjustments were made. All waters with $B > 50$ Å^2 were removed (21 atoms) and all protein atoms with $B > 50$ Å^2 were set to zero occupancy (69 atoms). Over four more cycles fine adjustments were made to the structure, which resulted in an *R* factor of 15.4% (R_{free} = 19.0%). All side chains not present were added with sensible stereochemistry and zero occupancy. Finally, the R_{free}-flagged reflections were added to the refinement to yield a final *R* factor of 15.5%. The final model consisted of 2575 protein atoms (74 at zero occupancy), 187 waters and two Cu atoms. The Ramachandran plot shows 90.9% of residues to be in the core regions, with the remaining 9.1% in the additionally allowed regions. *REFMAC* gave an overall coordinate estimated standard uncertainty (ESU) of 0.12 Å (based on the R_{free} value) and a *B*-factor ESU of 2.9 Å^2. Details of the refinement statistics can be found in Table 2.

2.8.2. Recombinant structure. The rcNiR model was subjected to a cycle of positional and individual *B*-factor refinement in *REFMAC* using data in the resolution range 20.0–1.9 Å. This resulted in an *R* factor of 18.3% (R_{free} 20.6%). The model consisted of 2528 protein atoms, 87 waters, a 0.25 occupancy Cu atom in the type 1 Cu site and a 0.25 occupancy Zn atom in the type 2 Cu site. A round of water selection followed, in which it was noted that a water was ligated to the type 2 site Zn. This was refined as a 0.25 occupancy atom, but this yielded a *B* factor of 4.1 Å^2 for the water compared with 19.3 Å^2 for the Zn atom. Given the very weak anomalous peak

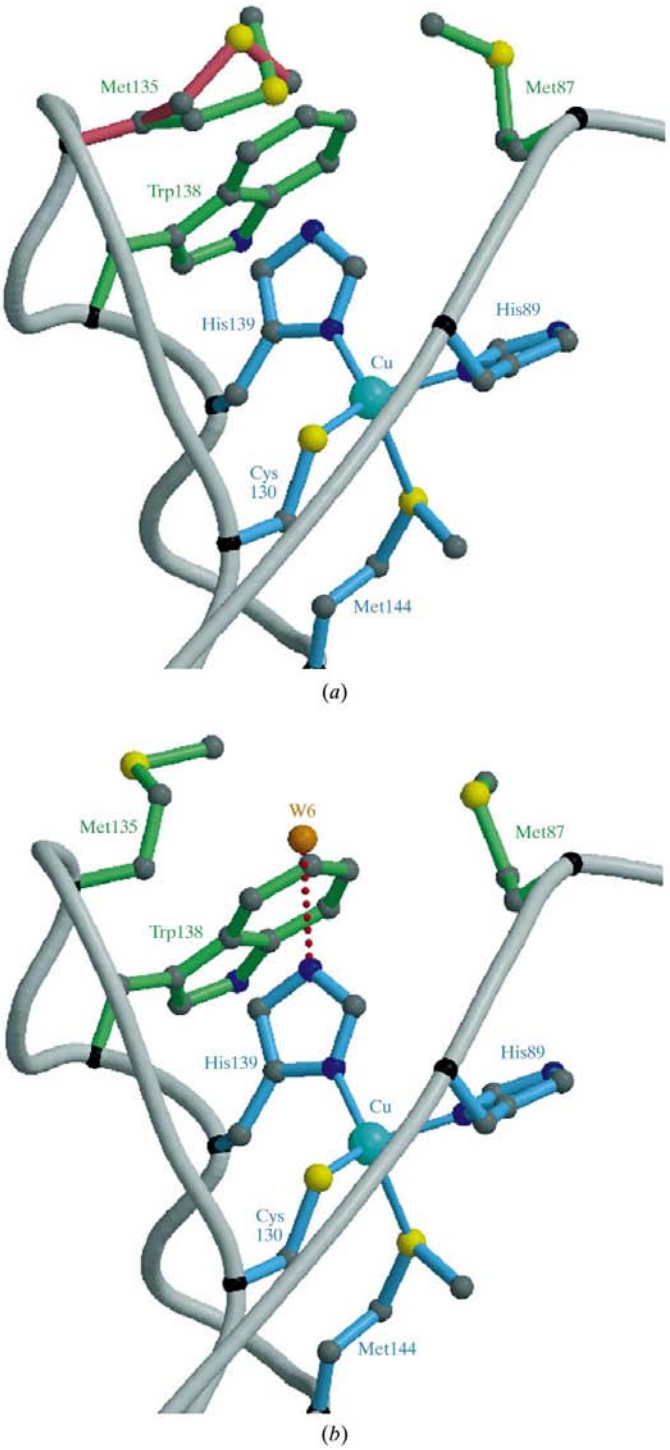

Figure 2
The type 1 Cu site (blue) and the surface hydrophobic residues (green) of (*a*) ntNiR and (*b*) rcNiR. The surface above the type 1 Cu site in ntNiR is in a closed conformation. The disordered Met135 (dual conformations shown in red and green) and Met87 cover the type 1 Cu site. In rcNiR, Met135 and Met87 both adopt single conformations which lead to an opening of the surface and the binding of a water (W6) to His139 $N^{\varepsilon 2}$. A water found in this position in the cupredoxin azurin is associated with electron transfer into the type 1 Cu site (Baker, 1988; Dodd *et al.*, 1995).

for the Zn atom in the type 2 site a water was placed there instead at full occupancy and refined along with the second (ligating) water, again at full occupancy. Both water molecules refined satisfactorily, with respective *B* factors of 16.9 and 28.9 Å^2. The *B* factor of water occupying the type 2 Cu site is close to that of the ligating atoms. Attempts to refine low-occupancy Zn in the type 2 site failed to give satisfactory results. The type 1 Cu site refined well with the 0.25 occupancy Cu to a *B* factor of 23.4 Å^2, again similar to the ligating atoms. Subsequently, three more cycles of fine adjustments were made to the structure, which resulted in an *R* factor of 17.1% (R_{free} = 20.0%). Finally, the R_{free}-flagged reflections were added to the refinement to yield a final *R* factor of 17.2%. All side chains not present were added with sensible stereochemistry and zero occupancy. The final model consisted of 2575 protein atoms (124 at zero occupancy), 149 waters and one Cu atom at 0.25 occupancy. The Ramachandran plot shows 89.9% of residues to be in the core regions, with the remaining 10.1% in the additionally allowed regions. *REFMAC* gave an overall coordinate ESU of 0.12 Å (based on the R_{free} value) and a *B*-factor ESU of 2.2 Å^2. Details of the refinement statistics can be found in Table 2.

Table 3
Copper-site geometry.

	Low-pH NiR, 2.1 Å	ntNiR, 1.9 Å	rcNiR, 1.9 Å
Type 1 site distances (Å)			
Cu—His89 $N^{\delta1}$	2.07	2.06	2.03
Cu—His139 $N^{\delta1}$	1.94	1.97	2.05
Cu–Cys130 S^{γ}	2.21	2.18	2.11
Cu—Met144 S^{δ}	2.62	2.68	2.57
Cu—Pro88 O	4.09	4.09	4.24
Type 1 site angles (°)			
His89 $N^{\delta1}$—Cu—His139 $N^{\delta1}$	102.7	98.3	97.0
His89 $N^{\delta1}$—Cu—Cys130 S^{γ}	127.1	129.7	122.2
His89 $N^{\delta1}$—Cu—Met144 S^{δ}	85.7	84.1	88.1
His139 $N^{\delta1}$—Cu—Cys130 S^{γ}	116.9	118.2	120.3
His139 $N^{\delta1}$—Cu—Met144 S^{δ}	115.0	116.3	115.8
Cys130 S^{γ}—Cu—Met144 S^{δ}	105.8	106.3	109.1
Type 1 Cu planar displacement†	0.45	0.44	0.99‡
Type 2 site distances (Å)			
Cu—His94 $N^{\varepsilon2}$	2.07	2.02	2.07
Cu—His129 $N^{\varepsilon2}$	2.17	2.06	2.27
Cu—His300 $N^{\varepsilon2}$	2.17	2.06	2.10
Cu—Wat503A	2.26§	1.73¶	1.86
Cu—Wat503B	—	2.34¶	—
Type 2 Cu planar displacement††	0.80	0.91	0.73‡‡

† Displacement from the His89 $N^{\delta1}$—His139 $N^{\delta1}$—Cys130 S^{γ} plane towards Met144 S^{δ}. ‡ Displacement from the His94 $N^{\varepsilon2}$—His129 $N^{\varepsilon2}$—His300 $N^{\varepsilon2}$ plane towards Wat503A/B. § Chloride ion. ¶ Quarter occupancy. †† Half occupancy. ‡‡ Water oxygen.

3. Results and discussion

3.1. The high- and low-pH structures

The general structure of ntNiR at pH 8.5 remains unchanged from the pH 5.2 model (Dodd *et al.*, 1998). The type 1 Cu site is very similar to the low-pH structure, with no significant changes in the ligand position (Table 3). As in the low-pH structure, Met135, the residue between the His139 type 1 Cu ligand and the molecular surface, shows disorder. This has been modelled as a dual conformation (Fig. 2*a*). The type 2 Cu site (Table 3, Fig. 3) has been modelled with two half-occupancy waters (A503A and A503B) ligating the Cu. The omit map clearly shows the presence of these waters (Fig. 3). They are at distances of 1.73 and 2.35 Å, respectively, from the copper and have been interpreted as a hydroxyl ion and a water in view of their distances. The absence of the chloride found in the low-pH structure was unexpected since the crystallization medium contains 0.1 *M* $MgCl_2$ and Tris–HCl.

The His—Cu ligand distances of the type 2 Cu site are all shortened in the high-pH structure, consistent with a slight contraction of the Cu coordination owing to the presence of a smaller exogenous ligand as observed in previous EXAFS studies (Strange *et al.*, 1995). The absence of the chloride ligand coupled with the presence of a short Cu—O bond at the type 2 Cu is consistent with a hydroxyl ion being the exogenous ligand. Comparative ENDOR, EXAFS and crystallographic studies of *Ax*NiR have shown that the binding of nitrite to the oxidized type 2 Cu site results in the displacement of a bound water or hydroxyl ion (Dodd *et al.*, 1997, 1998; Howes *et al.*, 1994; Strange *et al.*, 1999). This displacement reaction appears to be important in the catalytic mechanism, since reduction of this site results in the loss of this exogenous ligand and loss of activity (Strange *et al.*, 1999). This centre in crystals of reduced *Af*NiR in the presence of nitrite shows a low occupancy in X-ray studies (Murphy *et al.*, 1997) and EXAFS of *Ax*NiR shows the reduced-type Cu centre is unable to bind the inhibitor azide (Strange *et al.*, 1999). EPR studies of nitrite binding show that the affinity of the site for substrate decreases with increasing pH

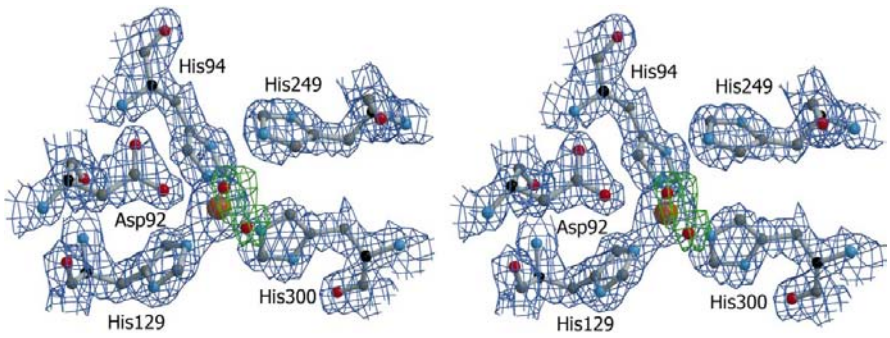

Figure 3
The stereo electron density of the type 2 Cu site residues (purple), contoured at 1σ. The omit difference density (contoured at 4σ) of the two partial occupancy waters (red spheres) is clear (green). The type 2 Cu is shown as an orange sphere.

(Abraham *et al.*, 1997). The data presented here showing that at high pH the site is occupied by a hydroxyl ion suggest that the lower affinity of the site for substrate is a consequence of the inability of nitrite to displace this ligand. This is consistent with the active species in NiR catalysis being an oxidized type 2 Cu centre with bound water as the exogenous ligand and would explain the rapid decrease in activity observed in *Ax*NiR above pH 6.0, which falls to negligible levels at pH 8.0 (Abraham *et al.*, 1997). This may be of general relevance to other NiRs since similar activity profiles have been determined for *Af*NiR (Kakutani *et al.*, 1981) and NiR from *Baccillus halodenitrificans* (Denariaz *et al.*, 1991). In a pH-dependence study (Adman *et al.*, 1995) no changes were found except in the occupancy of the type 2 Cu.

The water network identified in the low-pH structure, a suggested route of proton transfer to the type 2 Cu site, remains intact. This network runs along the monomer–monomer interface, beginning at Asp92, and continues *via* the imidazole of His254, reaching the surface of the molecule at Asp121 (Dodd *et al.*, 1998). A second water network extending from the front of the type 2 cavity has become clear in the current structure at least in part as a consequence of improved resolution. This second network leads from Asp92 to the carbonyl group of Ala131 *via* two waters and then the surface *via* Asn90 and Asn107 (Fig. 4).

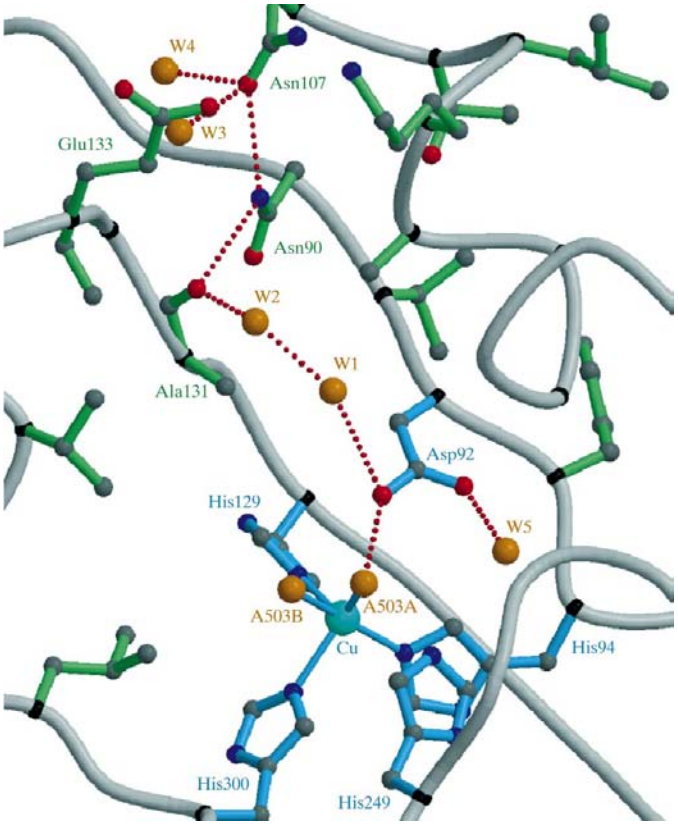

Figure 4
A second water hydrogen-bonded network (red dashes) extending from the front of the type 2 Cu cavity (blue residues) has been identified. This network leads from Asp92 to the carbonyl group of Ala131 *via* two waters (W1 and W2) and then the surface water (W3 and W4) *via* Asn90 and Asn107. The water network identified in the low-pH structure, a suggested route of proton transfer to the type 2 Cu site, remains intact. This network begins at W5 and extends to the right (Dodd *et al.*, 1998). The two partial occupancy waters (A503A and A503B) are also shown.

3.2. The structure of recombinant NiR – is the catalytic site devoid of metal?

The overall structure of rcNiR is again unchanged from the pH 5.2 model of the ntNiR, except that the first four N-terminal residues and the C-terminus were poorly defined ($B > 50$ Å^2) and have not been modelled. Both metal sites of rcNiR show low occupancy. This is unexpected given that the X-ray fluorescence and trace-metal analysis both showed a substantial quantity of Zn in the protein.

Comparison of the Cu *Kα* absorption edge XANES of the rcNiR with those of the oxidized and reduced native protein shows that Cu is present only in the type 1 site in rcNiR and that it is in the reduced form (Fig. 5). This is consistent with the crystals being colourless although the protein was initially blue. The anomalous maps and electron density show Cu in this site at ∼25% occupancy (Fig. 1). Anomalous maps suggest absence of Cu in the type 2 Cu site with only a trace amount of Zn present in this site. The Met135 side chain is now more well defined than in ntNiR, but is oriented away from His139. The side chain of Met87 is also found in a different conformation than in ntNiR. This leaves a surface cavity open, in contrast with the ntNiR, with a water bound (W6) to His139 $N^{\varepsilon 2}$ (Fig. 2*b*). A water found in this position in the cupredoxin azurin has been associated with electron transfer into the type 1 Cu site (Baker, 1988; Dodd *et al.*, 1995).

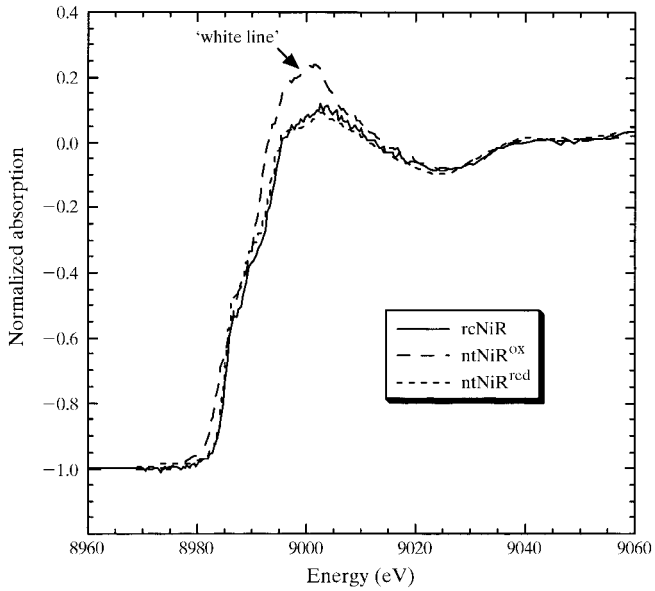

Figure 5
A comparison is made of the Cu *Kα* absorption edge of rcNiR with a reference spectra of the oxidized and reduced type 1 Cu site of ntNiR. The absence of the enhanced 'white-line' feature at the rcNiR absorption edge shows that the Cu is reduced.

The type 2 Cu site has been modelled with a water replacing the metal, as only a very weak Zn anomalous signal has been observed but the ligated water (A503) appears to have a full occupancy. The second water network from Asp92 *via* Ala131 identified in the high-pH form of ntNiR is also present in rcNiR. The EXAFS data on protein in solution suggest that Zn occupies the type 2 Cu site. Comparison with the Zn *K*-edge EXAFS of CuZn superoxide dismutase (SOD) suggests at least three histidine ligands bound to the Zn (Fig. 6). This is evidently not the case in the crystal structure, since neither the anomalous signal nor the electron density shows this. Adventitiously bound Zn at the protein surface is inconsistent with the EXAFS results, as no suitable site with three histidines can be found in the structure. The second possibility is that the type 2 site contains a labile or weakly bound Zn in the site and that most of it comes out during crystallization. This is surprising given the similarity of the type 2 Cu site to the Zn site of carbonic anhydrase (Strange *et al.*, 1995), which would have suggested that this metal should fit well into this site.

We have previously noted the close structural similarity between the Zn site of carbonic anhydrase (Eriksson *et al.*, 1988) and the catalytic Cu site of NiRs (Strange *et al.*, 1995). In carbonic anhydrase, the three ligated histidines and the catalytic water superimpose with those of NiR (see Fig. 2 in Strange *et al.*, 1995). The water molecule in carbonic anhydrase is held in position by the so-called 'doorkeeper' residue Thr199 and two other water molecules (Liljas *et al.*, 1994). Asp92 in NiR is ideally poised to provide similar anchoring to the ligated water molecule. We note, however, that carbonic anhydrase does not have a structural counterpart to the His249 of *Ax*NiR. Despite the close similarity between the two proteins with regard to the site geometry, the type 2 Cu-depleted NiR (T2DNiR) showed no detectable carbonic anhydrase activity. This lack of carbonic anhydrase activity is consistent with our finding that the site remains unoccupied in the crystal, despite the availability of zinc in the buffer and the crystallization medium. The crystallographic structures of the T2DNiR from *Achromobacter cycloclastes* also showed that the type 2 Cu site is occupied by water (Adman *et al.*, 1995). This strong preference for Cu in the catalytic site of NiR has also been demonstrated by a crystallographic study of a M150E mutant of *Af*NiR (Murphy *et al.*, 1995). Using the anomalous scattering signals of Cu and Zn, the type 1 site was found to be occupied by Zn with no metal detectable in the type 2 Cu site. It is likely that the enzyme has controls in place to ensure that Zn, if it binds, is unable to bind strongly at the active site.

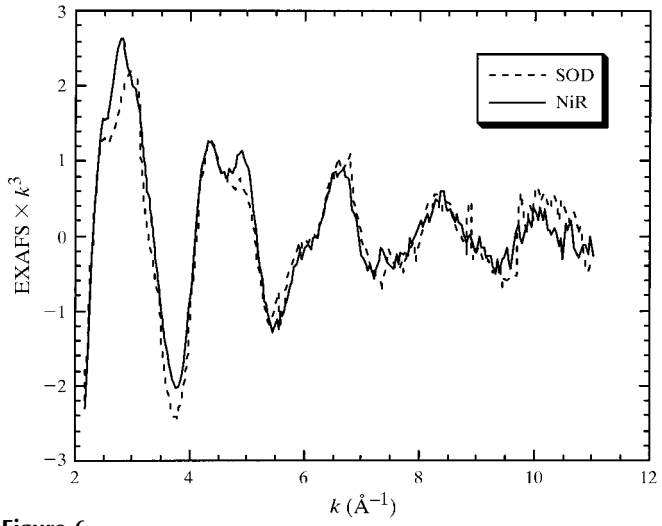

Figure 6
A comparison of the k^3-weighted Zn *K* edge EXAFS of rcNiR and CuZn SOD suggests at least three histidines ligate the zinc in rcNiR. This shows that in solution rcNiR the Zn must be in the type 2 Cu site, as no other site with suitable ligation exists within the protein.

3.3. Similarities with the catalytic site of superoxide dismutase

Purified preparations of NiR isolated from *Rhodopseudomonas sphaeroides* have been reported to have SOD activity (Michalski & Nicholas, 1985), but it is not known which copper centre has this activity. In order to clarify this point and examine the close similarity of the Cu site in the two enzymes, the superoxide dismutase activity of our preparations of T2DNiR and fully activated *Ax*NiR were measured and compared with bovine Cu_2Zn_2 SOD (Strange *et al.*, 1999). *Ax*NiR was found to have ∼56% of the bovine SOD activity, while T2DNiR did not exhibit any measurable activity.

In view of the activity data, we have further compared the structures of the type 2 Cu sites in *Ax*NiR and superoxide

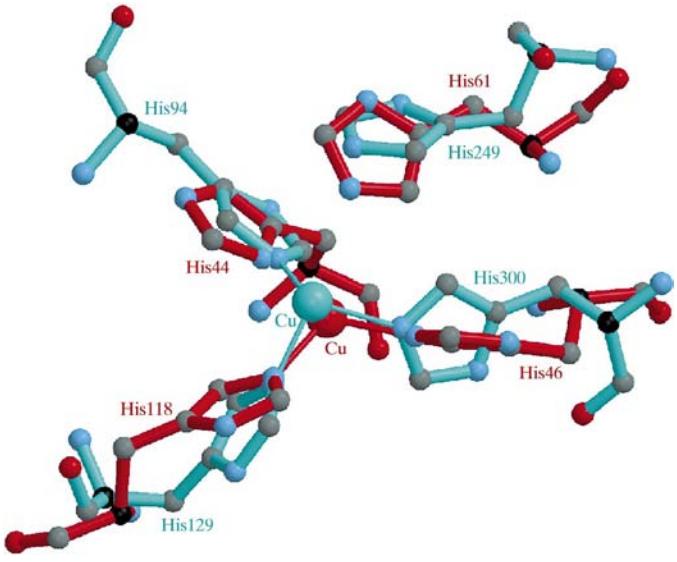

Figure 7
The coordination geometries at the type 2 Cu centres of *Ax*NiR (blue) and Cu site of bovine SOD (red) showing the structural similarity between them. In SOD His61, which links the Cu and Zn sites, is important in the catalytic cycle (Ogihara *et al.*, 1996). The residue has a similar position to His249 in NiR, which is a possible proton donor to the Cu site. Superposition was performed for three ligating atoms. The relative displacement of the Cu atoms results from NiR being oxidized and in SOD being reduced.

dismutase (Fig. 7). The type 2 copper site in oxidized *Ax*NiR shows almost tetrahedral geometry. In Cu_2Zn_2 SOD the Cu is pentacoordinate, with four histidine ligands in a plane and an apical solvent molecule. Recently, the crystal structure of yeast SOD has been determined in the reduced form (Ogihara *et al.*, 1996). This confirmed the structural rearrangement associated with the protonation of the imidazole residue (His61) bridging the Cu and Zn ions in the oxidized structure. The breaking of this imidazole bridge was again observed in a crystal structure of bovine SOD, where the two monomers show Cu sites in the oxidized and reduced forms (Hough & Hasnain, 1999). From a comparison of the Cu site in the reduced form of SOD with the oxidized structure of *Ax*NiR, a remarkable use of the same site is evident. His61 in Cu_2Zn_2 SOD adopts the same position as the unligated His249 of *Ax*NiR (Fig. 7).

4. Conclusions

The high-pH structure of ntNiR has provided a structural explanation for the rapid falloff in activity observed under alkaline conditions, with the presence of a hydroxyl bound to the type 2 Cu acting as an inhibitor of nitrite binding. The structure of the water network leading along the monomer–monomer interface in the low-pH structure (Dodd *et al.*, 1998) has been confirmed. The functional significance of the presence of the second water network is unclear, but we note that this network is only clearly visible in the pH 8.5 structure, which is at a slightly higher resolution (1.9 Å) than the pH 5.2 structure, which has been determined at 2.1 Å.

In the rcNiR structure lower occupancy of metal was found in both the type 1 and type 2 Cu sites. Crystallographic data collected at two wavelengths clearly showed that the type 1 Cu site contained copper to a level of 25% occupancy, consistent with the UV–visible and atomic absorption spectra and metal analysis. EXAFS showed this copper to be in the reduced oxidation state, which is consistent with the crystals being colourless, and implies that autoreduction has occurred. EXAFS clearly showed that Zn was present in a type 2 Cu-like coordination. Metal analysis and atomic absorption showed a Zn to Cu ratio of 5:1 in the protein in solution. The absence (or presence of only a trace amount) of Zn in the crystal structure is unexpected, especially as this site closely resembles the Zn site of carbonic anhydrase. If the protein in solution contains Zn in the type 2 Cu site, it must have a mechanism in place that prevents the Zn being tightly bound and consequently not being observed in the crystal structure.

This work was supported by the BBSRC/EPSRC Biomolecular Sciences programme (Grant 719/B06916 to SSH). The work in the laboratories of RRE and GS was supported by the BBSRC as part of a competitive strategic grant to the John Innes Centre. Figs. 1, 2, 3, 4 and 7 were produced with *Molscript* (Kraulis, 1991), *Bobscript* (Esnouf, 1997) and *Raster3D* (Merritt & Bacon, 1997).

References

Abraham, Z. H., Lowe, D. J. & Smith, B. E. (1993). *Biochem. J.* **295**, 587–593.
Abraham, Z. H. L., Smith, B. E., Howes, B. D., Lowe, D. J. & Eady, R. R. (1997). *Biochem. J.*, **324**, 511–516.
Adman, E. T., Godden, J. E. & Turley, S. (1995). *J. Biol. Chem.*, **270** 27458–27474.
Baker, E. N. (1988). *J. Mol. Biol.* **203**, 1071–1075.
Binsted, N. & Hasnain, S. S. (1996). *J. Synchrotron Rad.* **3**, 185–196.
Collaborative Computational Project, Number 4 (1994). *Acta Cryst.* D**50**, 760–763.
Denariaz, G., Payne, W. J. & LeGall, J. (1991). *Biochim. Biophys. Acta*, **1056**, 225–232.
Dodd, F. E., Hasnain, S. S., Abraham, Z. H. L., Eady, R. R. & Smith, B. E. (1995). *Acta Cryst.* D**51**, 1052–1064.
Dodd, F. E., Hasnain, S. S., Abraham, Z. H. L., Eady, R. R. & Smith, B. E. (1997). *Acta Cryst.* D**53**, 406–418.
Dodd, F. E., Van Beeumen, J., Eady, R. R. & Hasnain, S. S. (1998). *J. Mol. Biol.* **282**, 369–382.
Eriksson, A. E., Jones, T. A. & Liljas, A. (1988). *Proteins*, **4**, 274–282.
Esnouf, R. M. (1997). *J. Mol. Graph.* **15**, 132–134.
Godden, J. W., Turley, S., Teller, D. C., Adman, E. T., Liu, M. Y., Payne, W. J. & LeGall, J. (1991). *Science*, **253**, 438–442.
Grossmann, J. G., Abraham, Z. H. L., Adman, E. T., Neu, M., Eady, R. R., Smith, B. E. & Hasnain, S. S. (1993). *Biochemistry*, **32**, 7360–7366.
Grossmann, J. G. & Hasnain, S. S. (1997). *J. Appl. Cryst.* **30**, 770–775.
Hough, M. A. & Hasnain, S. S. (1999). *J. Mol. Biol.* **287**, 579–592.
Howes, B. D., Abraham, Z. H. L., Lowe, D. J., Brüser, T., Eady, R. R. & Smith, B. E. (1994). *Biochemistry*, **33**, 3171–3177.
Jones, T. A., Zou, J. Y., Cowan, S. W. & Kjeldgaard, M. (1991). *Acta Cryst.* A**47**, 110–119.
Kakutani, T., Watanabe, H., Arima, K. & Beppu, T. (1981). *J. Biochem.* **89**, 453–461.
Kraulis, P. J. (1991). *J. Appl. Cryst.* **24**, 946–950.
Kukimoto, M., Nishiyama, M., Murphy, M. E. P., Turley, S., Adman, E. T., Horinouchi, S. & Beppu, T. (1994). *Biochemistry*, **33**, 5246–5252.
Laskowski, R. A., MacArthur, M. W., Moss, D. S. & Thornton, J. M. (1993). *J. Appl. Cryst.* **26**, 283–291.
Liljas, A., Håkansson, K., Jonsson, B. H. & Xue, Y. (1994). *Eur. J. Biochem.* **219**, 1–10.
Merritt, E. A. & Bacon, D. J. (1997). *Methods Enzymol.* **277**, 505–524.
Michalski, W. P. & Nicholas, D. J. D. (1985). *Biochim. Biophys. Acta*, **828**, 130–137.
Miyahara, J., Takahashi, K., Ameniya, Y., Kamiya, N. & Satow, Y. (1986). *Nucl. Instrum. Methods A*, **246**, 572–578.
Morrell, C., Bilsborrow, R. L. & Derbyshire, G. E. (1989). Daresbury Laboratory Technical Memorandum DL/Sci/TM63E 1–12. Warrington: Daresbury Laboratory.
Murphy, L. M., Strange, R. W., Karlsson, G., Lundberg, L., Pascher, T., Reinhammar, B. & Hasnain, S. S. (1993). *Biochemistry*, **32**, 1965–1975.
Murphy, M. E. P., Turley, S. & Adman, E. T. (1997). *J. Biol. Chem.* **272**, 28455–28460.
Murphy, M. E. P., Turley, S., Kukimoto, M., Nishiyama, M., Horinouchi, S., Sasaki, H., Tanokura, M. & Adman, E. T. (1995). *Biochemistry*, **34**, 12107–12117.
Murshudov, G. N., Vagin, A. A. & Dodson, E. J. (1997). *Acta Cryst.* D**53**, 240–255.
Navaza, J. (1994). *Acta Cryst.* A**50**, 157–163.
Ogihara, N., Parge, H. E., Hart, P. J., Weiss, M. S., Goto, J. J., Crane, B. R., Tsang, J., Slater, K., Roe, J. A., Valentine, J. S., Eisenberg, D. & Tanier, J. A. (1996). *Biochemistry*, **35**, 2316–2321.

Otwinowski, Z. & Minor, W. (1997). *Methods Enzymol.* **276**, 307–326.
Payne, W. J. (1985) *Denitrification in the Nitrogen Cycle.* New York: Plenum.
Prudêncio, M., Eady, R. R. & Sawers, G. (1999). *J. Bacteriol.* **181**, 2323–2329.
Sakabe, N. (1991). *Nucl. Instrum. Methods A*, **303**, 448–463.
Strange, R. W., Dodd, F. E., Abraham, Z. H. L., Grossmann, J. G., Brüser, T., Eady, R. R., Smith, B. E. & Hasnain, S. S. (1995). *Nature Struct. Biol.* **2**, 287–292.
Strange, R. W., Murphy, L. M., Dodd, F. E., Abraham, Z. H. L., Eady, R. R., Smith, B. E. & Hasnain, S. S. (1999). *J. Mol. Biol.*, **287**, 1001–1009.
Zumft, W. G. (1997). *Microbiol. Mol. Biol. Rev.* **61**, 533–616.